Title	Molten salt synthesis of CoFe2O4 and its energy storage properties
Author(s)	Kulkarni, P., Balkrishna, R. G., Ghosh, D., Rawat, R. S., Medwal, R., Chowdari, B. V. R., Karim, Z., & Reddy, M. V.
Source	*Materials Chemistry and Physics, 2020*
Published by	Elsevier

The final publication is also available at: https://doi.org/10.1016/j.matchemphys.2020.123747

Molten salt synthesis of $CoFe_2O_4$ and its Energy Storage Properties

Pranav Kulkarni [1,2,5], R. Geetha Balkrishna [1*], Debasis Ghosh [1], R.S Rawat [2**], Rohit Medwal [2], B.V.R. Chowdari [4], Zaghib Karim[6], M. V. Reddy [3,5,6 ***]

[1] Centre for Nano and Material Sciences, Jain University, Jain Global Campus, Kanakapura, Ramanagaram, Bangalore, 562112, India.

[2] Natural Science and Science Education, National Institute of Education, Nanyang Technological University Singapore, Singapore.

[3] Department of Materials Science and Engineering, National University of Singapore, Singapore 117575, Singapore.

[4] School of Materials Science and Engineering, Nanyang Technological University Singapore, Singapore.

[5] Department of Physics, National University of Singapore, Singapore, 117542.

[6] Centre of Excellence in Transportation Electrification and Energy Storage (CETEES), Hydro-Québec, 1806, Lionel-Boulet blvd., Varennes, Qc, J3X 1S1, Canada

Abstract:

In this article, we report simple and scalable one-pot molten salt synthesis of $CoFe_2O_4$ as electrode material for Lithium ion batteries. X-ray diffraction studies along with Rietveld analysis showed a pure phase of $CoFe_2O_4$ with space group *Fd-3m* and crystallite size of 54 nm. As an anode material $CoFe_2O_4$ showed high initial discharge/charge capacity of 1556/1093 mA h g^{-1} and a reversible capacity of 926 mA h g^{-1} after 30 cycles with columbic efficiency of 99 %. A relatively high reversible capacity of 594 mA h g^{-1} was observed at high current density of 1 C (916 mA g^{-1}) which shows the better reversibility of $CoFe_2O_4$ at high current density. As the current was reduced to 0.1 C reversible capacity of 899 mA h g^{-1} was retained suggesting high rate performance of $CoFe_2O_4$. The long-term stability test, carried out using galvanostatic charge/discharge (GC) at a current density of 0.5 C, showed a reversible capacity of 369 mA h g^{-1} at the end of 200^{th} cycle. The structural and morphological evaluation of the sample after cycling, using ex-situ X-ray diffraction and ex-situ transmission electron microscopy, confirmed structural degradation and formation of metal nanoparticles, Li_2O and amorphous nature of electrode material. The one-pot molten salt synthesis approach is quite simple and can be extended for large-scale production of electrode materials.

Key words: $CoFe_2O_4$, Molten salt synthesis, Lithium batteries, Anode, Ex-situ XRD, Ex-situ TEM, Impedance spectroscopy

Corresponding authors E-mail addresses:

*br.geetha@jainuniversity.ac.in (Geetha. Balakrishna),

**rajdeep.rawat@nie.edu.sg (R.S. Rawat),

*** reddymvvr@gmail.com, MogalahalliVenkatesh.VenkatashamyReddy@ireq.ca (M.V. Reddy).

1. Introduction:

Lithium ion batteries (LIBs) have been extensively used as crucial energy storage devices, from portable devices such as mobile phones, laptops, drones to hybrid energy vehicles (HEV)[1]. With the rapid progress of technologies, the demand for high energy density LIBs has increased in recent times [2]. The overall performance of LIB depends on anode, cathode and electrolyte [2,3, 4, 5, 6]. The cathode and electrolyte, usually contain trace amount of lithium, and serve as lithium source and transport carrier, respectively. Graphite has been widely used as anode material which undergoes intercalation reaction with lithium providing a theoretical capacity of 372 mA h g^{-1}, which constrains the LIB performance [1,7]. On the other hand, metal oxides and sulfides have been explored as potential electrode materials as they possess high theoretical capacities [5,8,9]. Metal oxides (MO) undergo conversion reaction with lithium to store the charge carries. Thus transition metal oxides with rich oxidation/reduction ability, are being widely explored [10-14]. In recent years, binary metal oxides such as AB_2O_4 (A= Co, Mn, Fe, Zn, and Ni; and B= Co, and Fe) have been investigated as electrode materials and have shown superior performances as each of the two metal ions can accept several electrons [15-22]. Although conversion based materials possess high theoretical capacity, but they also exhibit critical drawbacks in the form of voltage hysteresis, high volume expansion and pulverization leading to short cycle life that hinder the commercialization of conversion based electrodes [23]. In order to enhance the stability and conductivity of these metal oxides, conductive carbon have been widely explored as composite materials. Nanocomposites of these metal oxides with carbon or graphene have shown enhanced performance with better stability [24-26].

Electrochemical properties of spinel Co_3O_4 have been extensively studied as potential electrode materials for LIB due to their high redox ability of Co, but the high cost and toxicity of Co hinder its use as electrode material. To reduce the cost and toxicity of cobalt compounds various ternary metal oxides have been explored, of which $CoFe_2O_4$ (high theoretical capacity of 916 mA h g^{-1}) [27] has been greatly studied. Along with the high capacity, Fe is abundantly and cheaply available in Earth's crust and hence adds to the advantage of substituting Co by Fe in electrode material. Lavela *et al* synthesized $CoFe_2O_4$ by sol-gel method [28] which delivered a capacity of 600 mA h g^{-1} after 80 cycles. In another approach, sol-gel combustion was explored by Sagar *et al* [19] for the synthesis of $CoFe_2O_4$ and investigated the role of binder on the electrochemical

properties. Hwangbo *et al* utilized electrospinning method for the synthesis of $CoFe_2O_4$ nanofibers which showed a capacity of 660 mA h g^{-1} after 100 cycles[29]. In another attempt, Yoon *et al* [30] synthesized spherical $CoFe_2O_4$ by microwave-hydrothermal method that showed a capacity of 730 mA h g^{-1} after 50 cycles. $CoFe_2O_4$ nanotubes were synthesized by hydrothermal method by Zhang *et al* [31]. In order to enhance the stability of $CoFe_2O_4$, various strategies such as graphene composite formation[24, 28, 29, 32-36] and carbon coating [37] have been explored. A small amount of graphene/carbon can provide a conductive network and help in better conductivity and stability. In some cases, composite architectures such as $Co_3O_4/CoFe_2O_4$ [38], and $CoO/CoFe_2O_4$ [39] have also been explored as a potential electrode materials.

Although all these materials possess very high capacity, their usage seems limited mostly as it is difficult to extend these approaches to large scale production. Herein, we report a high yield and scalable approach for the synthesis of $CoFe_2O_4$ material that possesses comparable performance. In this article, we adopt the one-pot molten salt method for the synthesis of $CoFe_2O_4$ nanoparticles using NaCl and NaOH as eutectic salts, which are of low cost and are abundant in nature. The molten salt method has been explored as one of the simple method for the preparation of various metal oxides for energy storage and catalysis and other applications[40-51], when compared to solid state method in molten medium reactivity will be better and no mechanical mixing or repeated heating and obtained materials showed a interesting electrochemical properties [43-51]. Also for academic interest with molten salt approach we can study the effect salt and reaction temperature, time and other factors on morphology and structure and electrochemical properties of materials.

Experimental part:

2.1 Synthesis of $CoFe_2O_4$:

In a typical method, metal precursor such as $CoSO_4.7H_2O$ (Sigma Aldrich) and $FeSO_4.7H_2O$ (Fulka) were thoroughly mixed in 1:2 molar ratio with mortar and pestle. NaOH and NaCl were used as the molten salt in the molar ratio 8:10 and added to the precursor in a crucible. The crucible containing the material was then transferred to a box furnace and heated at 700 °C for 2 hours in air with the heating and cooling rate of 3 °C min^{-1}. After cooling the reaction mixture was washed with deionized water to remove the excess dissolved unreacted products followed by vacuum filtration. The obtained product was dried in an oven maintained at 80 °C. As synthesized

product were used for all characterization without any further treatment. A high yield of 91 % was obtained which shows the scalability of the synthesis approach. Although some amount of material was washed out during the washing process.

2.2 Material Characterization:

To understand the physical properties, synthesized compounds were characterized by X-Ray powder diffraction (XRD) using Cu K_α radiation (Bruker D8), scanning electron microscopy (SEM) using JOEL JSM-5600LV and Transmission electron microscopy (TEM) using JOEL JEM-2010F. X-ray photoelectron spectroscopy (XPS) was carried out using AXIS ultra DLD spectrometer (Kratos Analytica) with monochromatic Al K_α radiation. Charge referencing was carried out against adventitious carbon C (C 1s binding energy = 284.6 eV) and the data was analyzed using Casa XPS software. Brunauer–Emmett–Teller (BET) was carried out to investigate the surface area using ASAP 2010 (Micromeritics) instrument.

2.3 Preparation of Electrodes and Electrochemical Studies

To understand the electrochemical performance of $CoFe_2O_4$, CR2016 coin cells were fabricated. The electrode material was prepared by mixing 70 % of active material ($CoFe_2O_4$), 15 % of Super-P carbon and 15 % of polyvinylidene fluoride (PVDF). All the materials are finely ground in mortar and pestle followed by addition of N-Methyl-2-pyrrolidone (NMP) as a solvent to ensure better mixing and to obtain a homogeneous slurry. The homogeneous slurry obtained is spread over etched copper foil by using doctor blade technique. The coated copper foil is then transferred to an oven maintained at 80 °C until all the solvent is evaporated. Once the electrode material has dried up, the copper foil coated with electrode material was made to pass through a twin roller to obtain closer contact between the electrode material and the copper foil. Finally, the electrode material was cut into circular discs using the electrode cutter (mass loading = 2-3 mg). Before the fabrication of CR2016 coin cells, all the electrodes are dried in vacuum oven. CR2016 type coin cells were fabricated using $CoFe_2O_4$ as a positive electrode and Li metal as negative electrode separated by a polymer separator (Celgard-2400). 1 M $LiPF_6$ dissolved in the equal volumetric ratio of ethylene carbonate (EC) and dimethyl carbonate (DMC) was used as the electrolyte (Sigma Aldrich). The cells were assembled in an Argon filled glove box with H_2O and O_2 contents less than 1 ppm.

Electrochemical studies such as galvanostatic charge-discharge cycling (GC) were performed using Bitrode multi-channel tester (Model SCN-12-4/18, USA) and cyclic voltammetry (CV) were performed using Solartron 1470 battery test unit in the potential range of 0.005 - 3.0 V vs. Li at room temperature. Electronic impedance spectroscopy (EIS) was carried out using Solartron impedance analyzer (SI1255) in the frequency range of 0.35 MHz to 3 mHz with a AC amplitude of 10 mV.

2. Results and discussion

3.1 Structure and Morphology

The X-ray diffraction (XRD) pattern of as obtained $CoFe_2O_4$ nanostructures is shown in Fig.1. The XRD pattern shows the peaks centered at 30.47°, 35.84°, 37.49°, 43.5°, 54.00°, 57.44° and 63.09° corresponding to (022), (311), (222), (004), (422), (511) and (044) hkl planes, respectively. The observed Bragg peaks are well matching with the literature data on the crystal structure of $CoFe_2O_4$ [30, 52]. In order to understand the detailed crystal structure and to determine the lattice parameter of $CoFe_2O_4$, Rietveld refinement was performed using the TOtal Pattern Analysis System (TOPAS) software by considering the octahedral and tetrahedral position of both Co^{2+} and Fe^{3+} ions in space group *Fd-3m* (227).

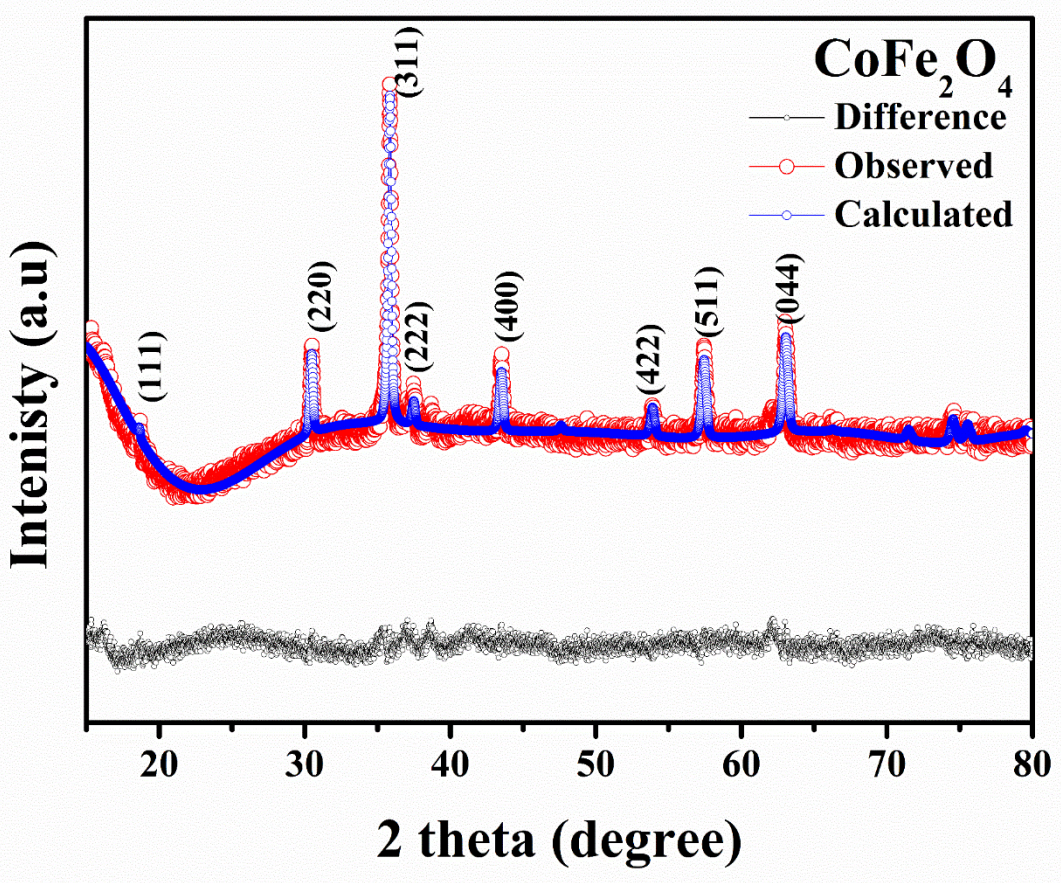

Fig.1. Experimental and profile fitted X-Ray diffraction pattern of as prepared $CoFe_2O_4$ NPs. Red and blue curves correspond to the experimental data and fitted profile curve whereas the black curve represents the difference between the experimental and fitted profile. All the Bragg peaks were indexed with respect to space group Fd-3m.

The Rietveld refinement pattern shows a reasonably good fit with experimentally observed XRD pattern of $CoFe_2O_4$. Lattice parameter was found to be, a = 8.3749(4) Å with the average crystallite size of 54 nm. The obtained lattice parameter is in good agreement with the reported literature.

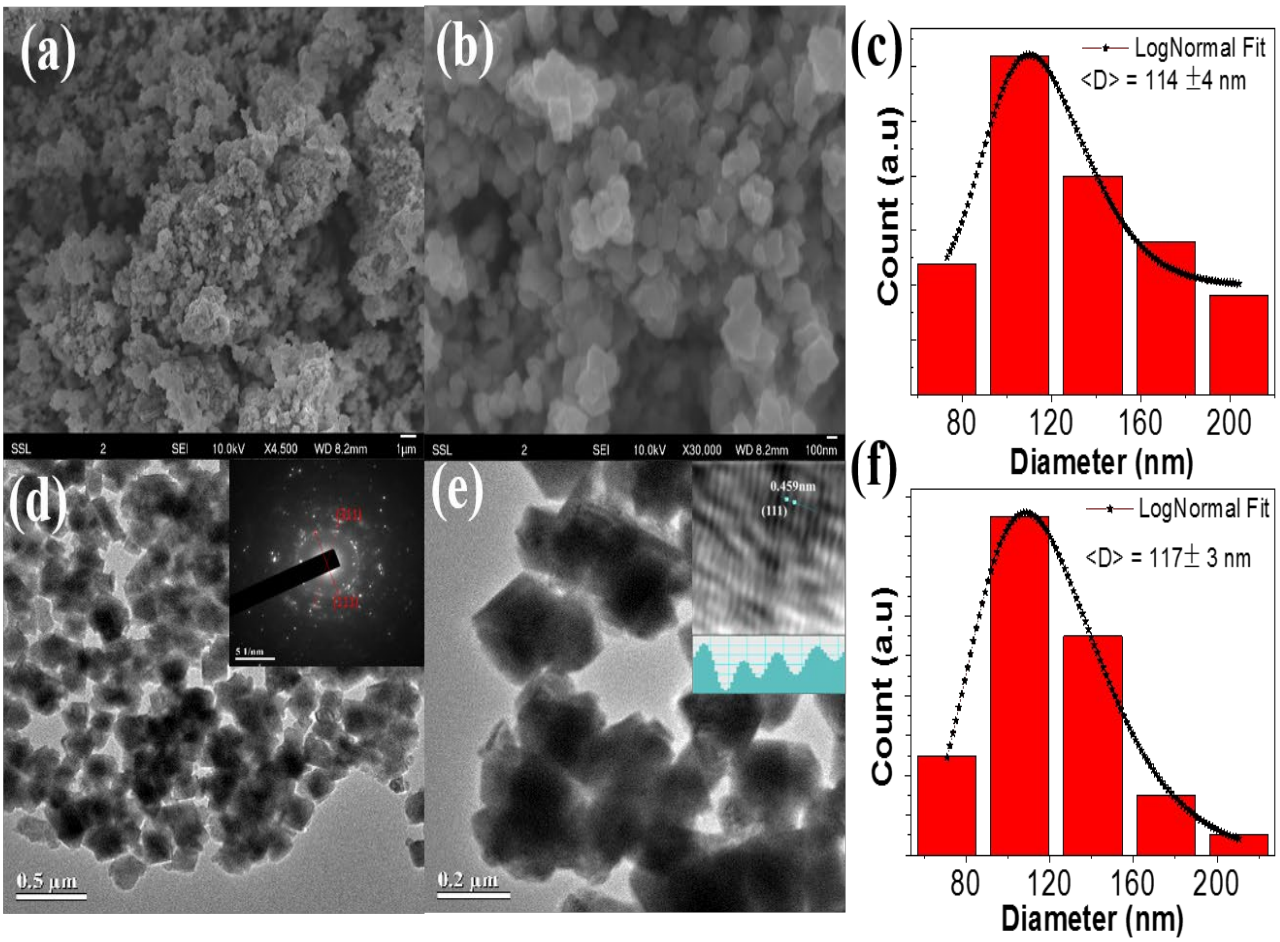

Fig 2. SEM images of $CoFe_2O_4$ NPs recorded at (a) low and (b) high magnification, (c) The particle-size distribution histogram, plotted from SEM image (a); (d, e) TEM images of the $CoFe_2O_4$ NPs at different magnifications. (f) Particle-size distribution histogram, estimated using the TEM image (d). Inset of the (d) and (e) shows the selected area electron diffraction and high-resolution Inverse Fast Fourier Transform (IFFT) images, respectively.

In order to understand the microstructure and morphology, scanning electron microscopy (SEM) and transmission electron microcopy (TEM) were carried out for the as prepared $CoFe_2O_4$. Fig 2 (a) and (b) show the SEM images of $CoFe_2O_4$ NPs recorded at low and high magnifications. It can be clearly seen that the as synthesized $CoFe_2O_4$ has mostly cubic morphology with average particle size of 114 ± 4 nm (Fig 2 (c)) as measured from Image J® software. The average particle size was

calculated by fitting the histogram using lognormal distribution as shown in Fig 2 (c). TEM measurement was also performed and the micrographs are as shown in the Fig 2 (d) and (e). TEM analysis shows the average particle size of 117 ± 3 nm which matches well with the SEM results within the particle size deviation range. Lattice fringes (shown in inset of Fig 2 (e)) of $CoFe_2O_4$ indicates an inter-planer spacing of 0.459 nm which belongs to the (111) plane with cubic structure as shown in the inset of Fig 2 (e) which is in good agreement with the XRD data. To further investigate the structure of $CoFe_2O_4$, selected area electron diffraction (SAED) was performed on $CoFe_2O_4$ NPs. The electron diffraction pattern is shown in the inset of Fig 2 (d). From the SAED pattern, inset of Fig. 2 (d), it can be seen that the obtained particles are polycrystalline in nature with reflections of (111) and (311) planes indexed. To further investigate the specific surface area of $CoFe_2O_4$, BET nitrogen adsorption-desorption analysis was carried out which exhibited a type III isotherm (Fig not shown). The surface area was calculated to be 8.01 m^2/g, which suggests the formation of pores during the washing of the as synthesized $CoFe_2O_4$.

The X-ray photoelectron spectroscopy (XPS) was used for the identification of site-specific oxidation states in the $CoFe_2O_4$ system. The core level spectra of C 1s, O 1s, Co2p and Fe 2p are shown in Fig.3. The core level scan of Co 2p show (Fig.3a) the presence of $2p_{3/2}$ and $2p_{1/2}$ peaks at 779.9 eV and 794.8 eV respectively with an energy difference of 14.9 eV confirming the presence of Co^{2+} valance states. Two peaks observed at 788.03 eV and 803.36 eV are the satellite peaks for Co $(2p)_{3/2}$ and Co $(2p)_{1/2}$ respectively. The Fe (2p) spectra shown in Fig. 3 (b) exhibits two binding energy peaks of Fe $(2p)_{3/2}$ at 710.6 eV and of Fe $(2p)_{1/2}$ at 724.1 eV, along with corresponding satellite peaks at 717.73 and 732.50 eV confirming the presence of Fe^{3+} valence state in $CoFe_2O_4$ [53]. Gaussian fitting of asymmetric Fe $(2p)_{3/2}$ peak results in two peaks centered at 710.2 eV and 712.5 eV corresponding to the Fe^{3+} in both octahedral and tetrahedral sites, respectively. On the other hand, core level spectra of O (1s), result in the two peak centered 529.6 eV and 530.6 eV (Fig 3 (c)). The peak observed at 529.6 eV is attributed to the contribution of the metal-oxygen bonding in crystal lattice and the binding energy at 530.6 eV may attribute the presence of the surface oxygen [53, 54].

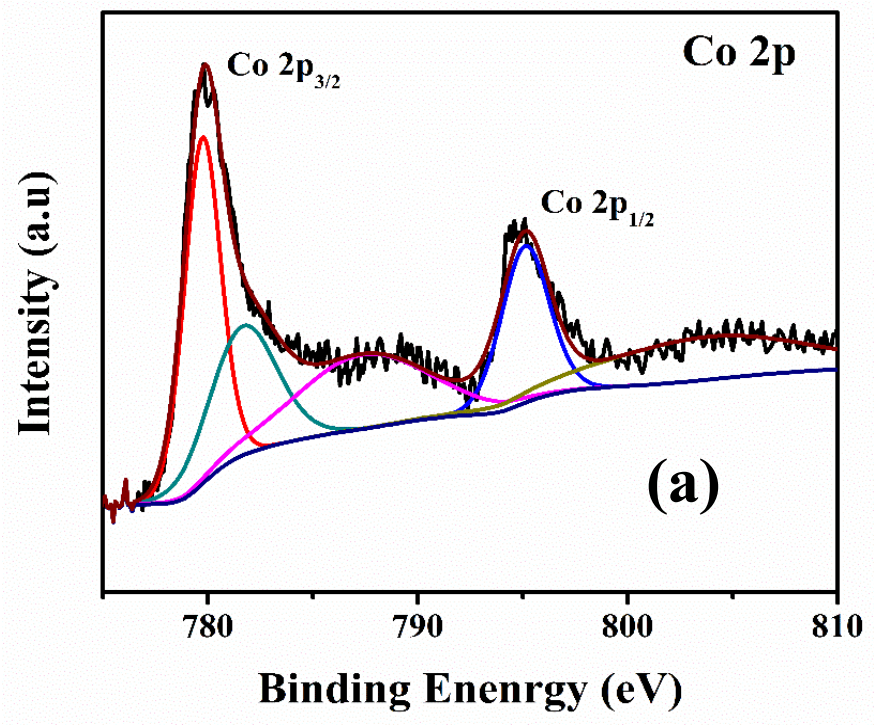
Co 2p
Co 2p3/2
Co 2p1/2
Intensity (a.u)
(a)
780
790
800
810
Binding Enenrgy (eV)

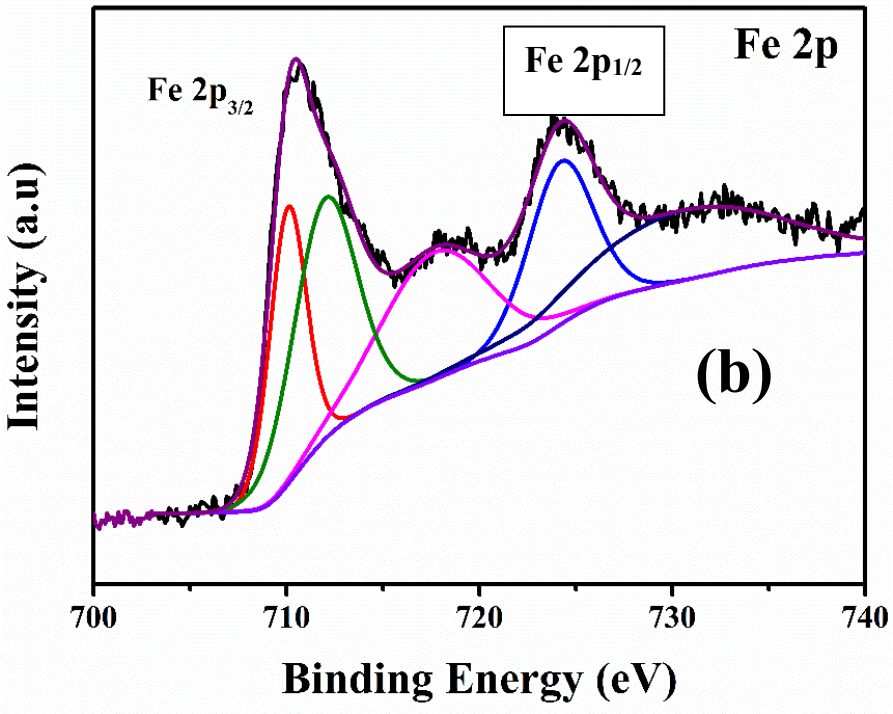
Fe 2p
Fe 2p3/2
Fe 2p1/2
Intensity (a.u)
(b)
700
710
720
730
740
Binding Energy (eV)

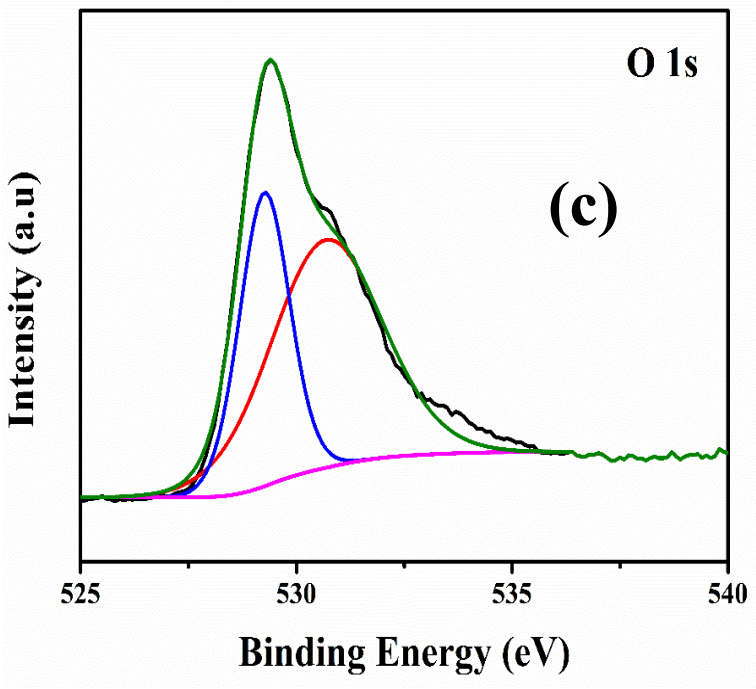

Fig. 3. X-ray photoelectron spectroscopy (XPS) spectra with Core shell spectrum of $CoFe_2O_4$ (a) Cobalt (Co 2p), (b) Iron (Fe 2p), and (c) Oxygen (O 1s).

3.2 Electrochemical Properties:

In order to understand the electrochemical reaction mechanism, cyclic voltammetry (CV) was carried out in the potential range of 0.005 – 3.0 V vs. Li at a scan rate of 0.1 mV s^{-1} for 5 cycles. Lithium metal was used as reference and counter electrode. Fig 4 shows the cyclic voltammetry of $CoFe_2O_4$ electrode for 1st, 2nd and 5th cycles respectively. In the first cathodic scan, the sharp reduction peak at 0.58 V are due to the electrolyte decomposition and formation of SEI during the first cycle. However, in the subsequent cathodic scans, the sharp peaks at 0.58 V disappears and two new peaks at 0.78 V and 1.42 V appear, which can be attributed to the reductive reaction of

Fe_2O_3 and CoO [55]. During the anodic scan, two small peaks are observed at 1.75 V and 2.20 V correspond to the oxidization reactions of Fe^0 and Co^0 to Fe^{3+} and Co^{2+} [27, 28]. From second and subsequent cycles, the cathodic and anodic scan have overlap of Co and Fe peaks resulting in broad region as shown in the Fig 4. Broad peaks in CV indicates structural degradation of the active material, similar peak broadening was observed in other spinel oxides [56, 57]. After five cycles the reduction and the oxidation are still prominent indicating good reversibility of the electrode material. Reactions presented in Equations (2) and (3) represent reversible reaction after the 1st cycle, which is quasi-irreversible in nature [27, 58]. In order to understand the rate capability and cycle stability of $CoFe_2O_4$, galvanostatic cycling was carried out.

$$CoFe_2O_4 + 8Li^+ + 8e^- \rightarrow Co + 2Fe + 4Li_2O \quad \text{--------- (1)}$$

$$Co + Li_2O \leftrightarrow CoO + 2Li^+ + 2\,e^- \quad \text{--------- (2)}$$

$$2Fe + 3Li_2O \leftrightarrow Fe_2O_3 + 6Li^+ + 2\,e^- \quad \text{---------- (3)}$$

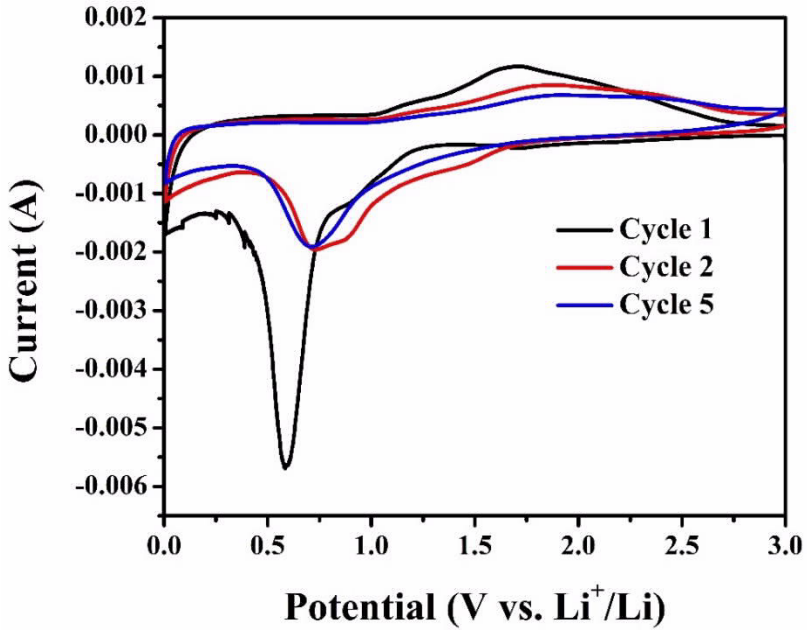

Fig. 4. Cyclic voltammetry of $CoFe_2O_4$ in the voltage range of 0.005-3.0 V vs. Li at a scan rate of 0.1 mV sec^{-1}.

Galvanostatic charge/discharge (GC) cycling study was carried out at a current density of 85 mA g^{-1} in the voltage range of 0.005 – 3 V; and the GC curves for 1st, 2nd, 30th and 50th cycles are shown in Fig 5 (a). The fabricated cells showed an open circuit voltage of 3.0 V. During the first

discharge cycle, there is a sudden decrease of voltage from 3 V to 1.5 V followed by another steep slope till 1.0 V which constitutes a capacity of 100 – 125 mA h g^{-1} and is attributed to the formation of $Li_xCoFe_2O_4$ intermediate. A flat voltage plateau is observed form 1 V to 0.5 V due to a high capacity of 1000 mA h g^{-1} followed by slow decrease to cut off voltage (0.005 V) which is mainly due to the reduction of metal oxides to its corresponding metal nanoparticles as shown in reaction 1 which leads to structure destruction. At the end of first discharge cycle, capacity of 1556 mA h g^{-1} was observed, which is 1.69 times the theoretical capacity of $CoFe_2O_4$. During the first charge cycle, a reversible capacity of 1093 mA h g^{-1} was obtained with a columbic efficiency of 70 %. During the first cycle an additional capacity is observed due to the reduction of solvent in the electrolyte and also due to the formation of solid electrolyte interface (SEI) which is observed in all conversion-based anode materials.

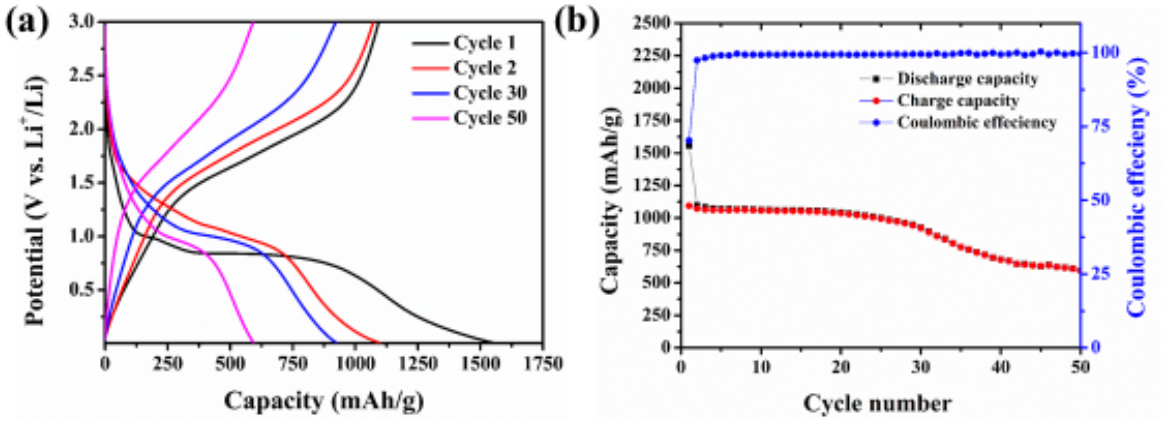

Fig.5. (a) Galvanostatic cycling studies at 1st, 2nd, 30th and 50th cycle at current density of 85 mA g^{-1}, and (b) capacity vs number of cycles and columbic efficiency of $CoFe_2O_4$.

In the subsequent cycle the reversible capacity of 1100 mA h g^{-1} was retained with columbic efficiency of 98 %. The capacity vs. cycle number are shown in Fig. 5 (b). During the first 30 cycles, 15 % capacity fading was observed with reversible capacity of 926 mA h g^{-1} at the end of

30^{th} cycle (with respect to 2^{nd} charge capacity). After 30^{th} cycle the capacity started to fade faster and reached a charge capacity of 594 mA h g^{-1} at the end of 50^{th} cycle with about 36% capacity fading from 30^{th} to 50^{th} cycle, with columbic efficiency of 99%. During the consecutive cycling, a rapid capacity fading was observed after the 30^{th} cycle. In conversion-based materials, all the active material is reduced to metal and Li_2O (Equation -1) and the prime reason behind the capacity fading is believed to be the irreversible conversion between the metal and metal oxide after many cycles. In addition to that the rapid capacity fading might also cause form the structural breakdown of $CoFe_2O_4$ and formation of amorphous particles. This could cause a loss in continuous electrical channel within the active materials and results in low active materials use during the process. This is further supported by our ex-situ TEM and XRD analysis of the cycled cell after 50 cycle after fully charging to 3 V. Both the TEM and XRD analysis indicated a change from polycrystalline to amorphous phase of the $CoFe_2O_4$ nanoparticles after 50^{th} GCD cycles. The detail analysis is discussed in coming section.

In order to understand the reversibility and rate capability of $CoFe_2O_4$ electrode, the coin cells were cycled at different current densities (0.1 C to 1 C where, 1 C = 916 mA g^{-1}) as shown in Fig 6 (a). At low current density of 0.1 C, a high average capacity of 950 mA h g^{-1} was obtained. When the current density was increased to 0.5 C, a reversible capacity of about 750 mA h g^{-1} was obtained. As the current density was further increased to 1 C (916 mA g^{-1}) a high reversible capacity of 540 mA h g^{-1} was obtained, much higher than the theoretical capacity of graphite (372 mA h g^{-1}), which suggests the better electrochemical activity of $CoFe_2O_4$ at high current density. As expected, as the current density increases there was slight reduction in reversible capacity. In order to investigate the reversibility, the current density was reduced to 0.5 C and 0.1 C and high reversible capacities of 627 mA h g^{-1} and 897 mA h g^{-1} were regained. Interestingly, at the end of 50^{th} cycle a high reversible capacity of 899 mA h g^{-1} was obtained at 0.1 C which shows the high reversibility of $CoFe_2O_4$ electrode. In order to test the long-term stability of $CoFe_2O_4$, galvanostatic charge/discharge was carried out at an intermediate discharge rate of 0.5 C for 200 cycles. As shown in Fig 6 (b), a high reversible capacity is obtained in the first few cycles which starts to reduce gradually and reaches a reversible capacity of 369 mA h g^{-1} at the end of 200^{th} cycle.

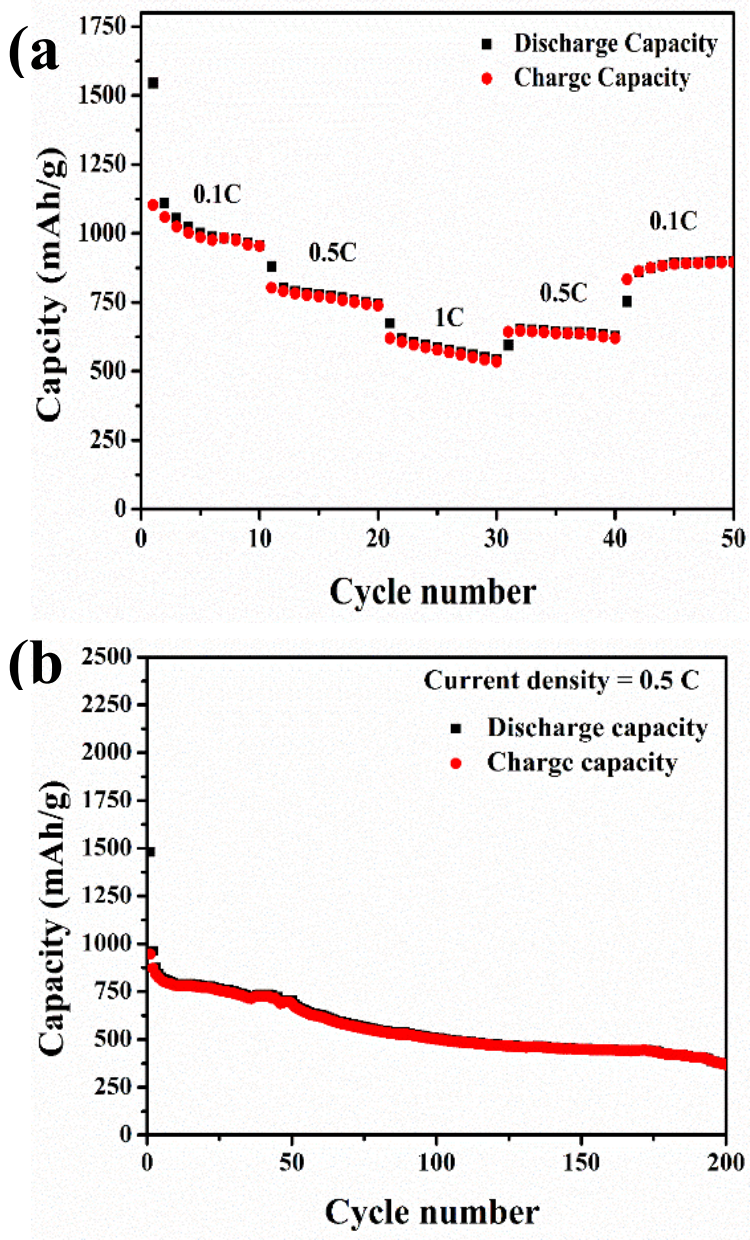

Fig.6. (a) Rate capability tests at various current densities, and (b) long term cycle stability of $CoFe_2O_4$ at a discharge current rate of 0.5 C.

In order to determine the electrochemical reaction and the reaction kinetics, electrochemical impedance spectroscopy (EIS) was carried out at different charge and discharge voltages. The open circuit voltage of the freshly fabricated cell was found to be 3.0 V. The program was created such that the cells were discharged at various voltages steps (2.5V, 2.0V, 1.5V, 1.0V, 0.5V, 0.005V) and relaxed for 1 h before running the EIS program. Similarly, the EIS data were obtained during charging (0.5V, 1.0V, 1.5V, 2.0V, 2.5V, 3V) and are represented in terms of Nyquist plot as shown in Fig. 7 and depending on semicircles the electrical circuit to fit the impedance plots are also shown in fig 7. Fresh cell showed a single semi-circle at 3.0V with an overall impedance of 368 Ω in the high to medium frequency range which can be attributed to combination of surface film and charge transfer resistance (R(sf +ct) as shown in Fig 7 and The equivalent circuit is as shown below Fig.7a . The electrolyte resistance (R1) is of order 4 to 7 ohms during discharge and charge cycle. The fitted impedance values R(sf +ct) during discharge cycle at 2.5, 2.0, 1.5, 1.0, 0.5 and 0.005 V are 376, 372, 152, 220, 89 and 57 (±1) Ω and corresponding capacitance due surface film and double layer capacitance (CPE (sf+dl) are 11.9, 11.3, 12.4, 15.7, 38.9, 57.5 μF. The Rsf, ct are surface film resistance arises due solid electrolyte interface of electrolyte and Rct charge transfer arises due to electrode electrolyte interface and corresponding capacitance (surface film and double layer) values are of the order in μF [59,60]. Overall end of discharge (0.005) impedance reduces to 57 Ω and the decrease in the resistance suggests the structural degradation of $CoFe_2O_4$ into its metal nanoparticles which possess better conductivity. During charging, at the voltage 0.5 V a two distinct semicircles which is the combination of Rsf+ct of 48 (±1) Ω; and (CPE (sf+dl) : 40 μF; and bulk resistance (Rb) of 20 and CPEb : 30 mF, respectively. Bulk resistance arises mainly due to electronic conductivity of active material and ionic conductivity of electrolyte, binder and conducting carbon [59, 60]. As the voltage is further increased to 1 V (Rsf+ct of 302 (±1) Ω; and (CPE (sf+dl) : 15 μF; and bulk resistance (Rb) of 119 and CPEb : 45 mF, there is an increase in the resistance which arises due to the restructuring of metal oxides such as CoO and Fe_2O_3 which possess lower conductivity compared to the metal nanoparticles. At the end of 3 V, a high resistance of ~375 Ω is obtained which is close to the overall impedance obtained for a fresh cell. These results suggest the structural destruction of $CoFe_2O_4$ to Co and Fe nanoparticle during discharge which shows a decreased impedance at lower voltages. Further studies with different cycle number and also impedance studies with three electrode system are needed to give more detail reaction mechanism.

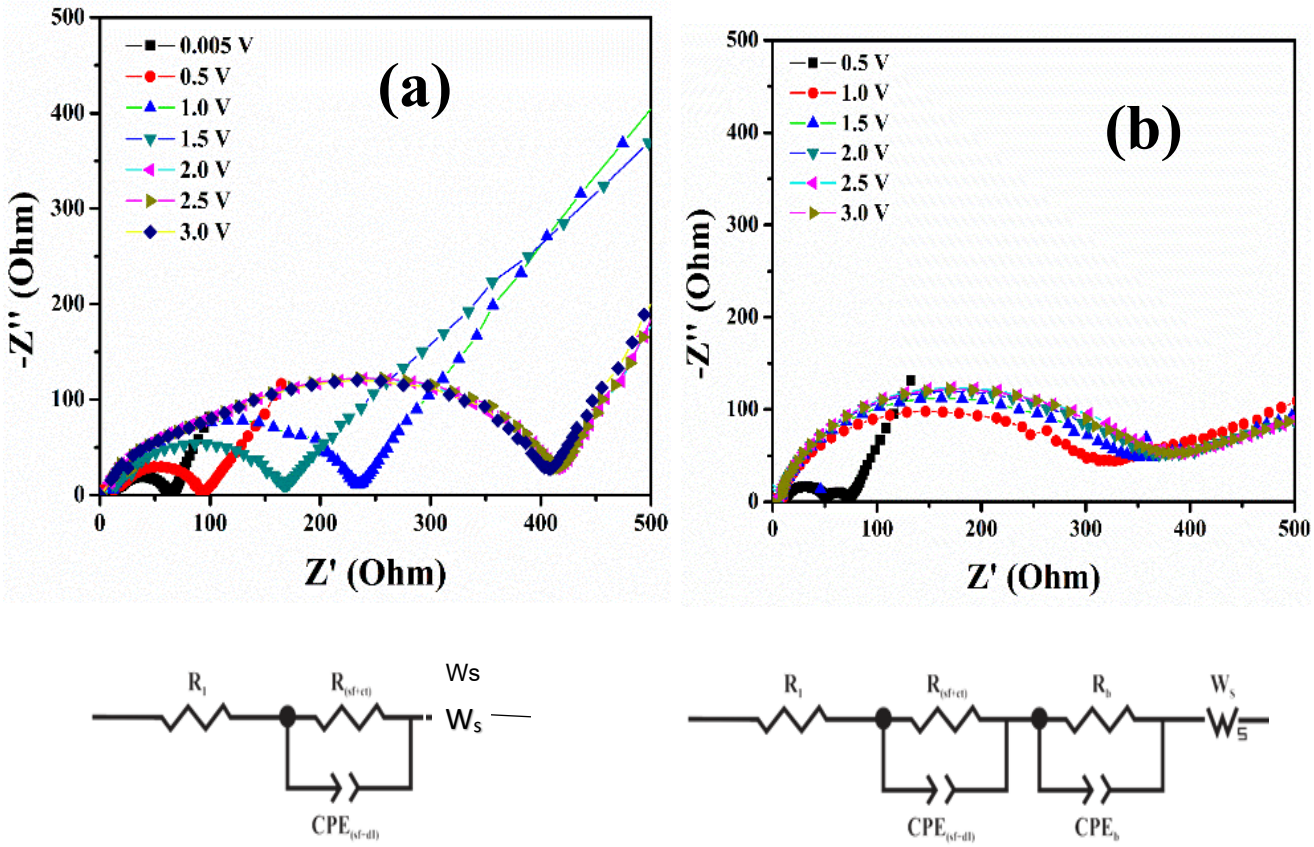

Fig.7. Electrochemical impedance spectroscopy studies of $CoFe_2O_4$. Nyquist plots (Z' vs. –Z'') for first (a) discharge cycle and (b) charge cycle at different voltages. Equivalent electrical circuit model fitted for (a) and (b) are also shown at bottom. R(st+ct): Surface film and charge transfer, Rb is bulk resistance, Ws is Warburg resistance and Constant phase element (CPE)sf, dl and b are capacitance due to surface film, double layer and bulk capacitance and R_1 Electrolyte resistance.

To further investigate the morphological effect of $CoFe_2O_4$ on the electrochemical cycling, Ex-situ TEM was carried out for the sample after 50th cycle as shown in Fig 8. The same cell was charged to 3.0 V and dissembled in the glove box and the electrode material was used for the TEM analysis. Fig 8 (a-b) shows the TEM images of $CoFe_2O_4$ after 50th cycle, which shows the

amorphous nature along with some amount of carbon which is expected in conversion-based electrodes. From SAED (selected area electron diffraction) pattern (Fig 8 (d)), it was observed that the material possessed circular fringes belonging to both CoO and Fe_3O_4 phase which are expected in the charge state according to the reactions in Equations (2) and (3). Fig 8 (c) and the inset of Fig 8 (c) shows the HRTEM and the line intensity plot of the cycle materials which shows the fringes with inter-planar spacing of 3.67 Å which is in close agreement with the inter-planar spacing of Fe_2O_3 with (012) plane confirming the formation of the reaction products in the mechanism.

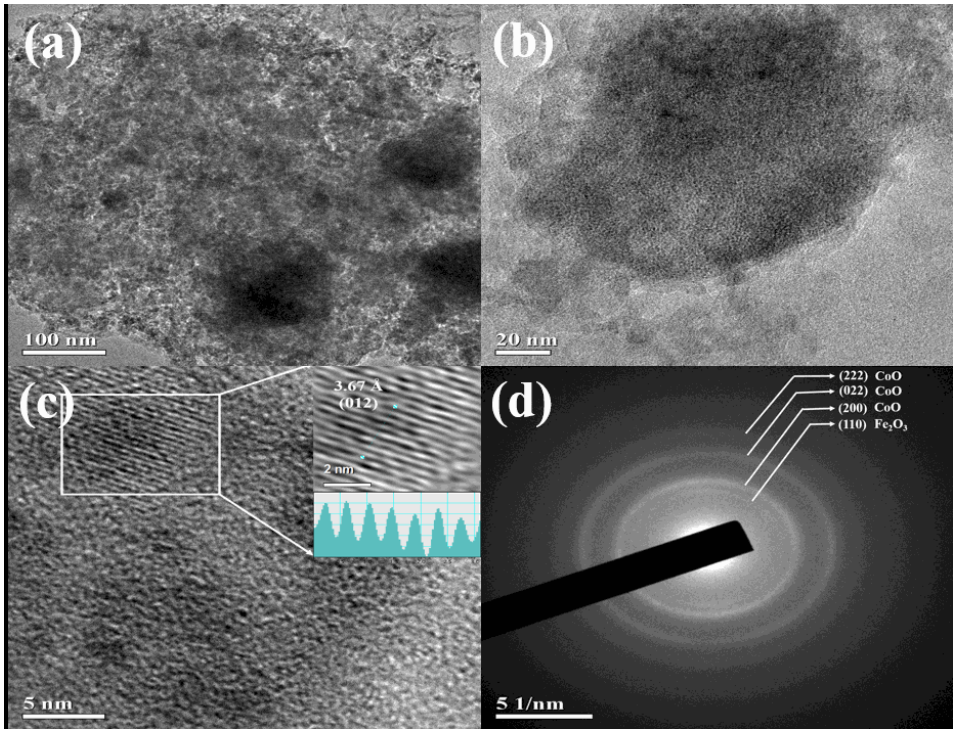

Fig. 8. Transmission electron microscopy (TEM) of $CoFe_2O_4$ after 50 cycling in the charged state, 3.0 V at (a) Low and (b) high magnification (c) High resolution TEM of $CoFe_2O_4$ (d) SAED pattern of $CoFe_2O_4$ after 50 cycles.

In order to understand the structural changes during the discharge/charge cycle, ex-situ XRD was carried out for $CoFe_2O_4$ electrode at various states of charge (1.5 V, 3 V) and discharge (0.005 V, 0.5 V, 1.5 V) and the XRD patterns are shown in Fig. 9. Test cells were charged/discharged at various voltages and dismantled in glove box and the electrode material were then analyzed for XRD. As the electrode material contained small amount of carbon along with the active material

not all the diffraction was prominent. Careful observation shows two major diffraction peaks for $CoFe_2O_4$ at about 30º and 35º which correspond to (220) and (311) planes as discussed in our XRD sections. When the cell was discharged to a voltage of 1.5 V, the cobalt ferrite structure was retained with slight peak broadening and shift to lower angle due to the strain induced on cobalt ferrite structure which suggest the reaction of Li with $CoFe_2O_4$ to form an intermediate nanostructure ($Li_xCoFe_2O_4$). As the discharge voltage is decreased to 0.5 V there is structural destruction which results in the formation of Li_2O (confirmed by a peak at 33º [61]) and metal nanoparticles (Co and Fe) with retention of (220) phase at 30º. The cells were studied for ex-situ XRD there is a possibility of formation of LiOH on the surface. As it is conversion-based material, $CoFe_2O_4$ structure is reduced to Fe and Co nanoparticles which are emended in Li_2O matrix. The amount of Fe and Co nanoparticles is small compared to Li_2O ($CoFe_2O_4 + 8Li^+ + 8e^- \rightarrow Co + 2Fe + 4Li_2O$) and are well dispersed in the Li_2O matrix, thus diffraction peaks are not prominent and could not be detected. Further into the deep discharge at 0.005 V, the presence of Li_2O diffraction peak was retained which are in good agreement with the reaction mechanism. This confirms the first step of electrochemical reaction proposed by reaction mechanism in electrochemical section. To understand the structural changes during charging, XRD was carried out at charged voltages of 1.5 V and 3.0 V. The cells were first discharged to 0.005 and charged to 1.5 V and analyzed, which shows the presence of Li_2O as shown in Fig 9 (a). At 1.5 V the conversion reaction (oxidation of metal to metal oxide) has not been initiated which is in good agreement with cyclic voltammetry. Interestingly, at 3.0 V no peak for Li_2O was observed, which suggest the complete removal of Li which is expected as per the reaction mechanism. This step suggests the complete reversible oxidation resulting in the formation of metal oxide as per the reaction mechanism (Equation 2 & 3). These results show the experimental evidence of structural destruction of cobalt ferrite and the formation of Li_2O during discharge and reveal the fundamental reaction mechanism observed in conversion-based electrodes. Although the formation of metal oxides is not prominent due to the amorphous nature, still it gives clear evidence on structural destruction on electrochemical cycling. To further understand the structure after cycling, XRD for cycled electrode was carried out, refer Fig 9 (b), which shows significant structural destruction with no diffraction peak observed suggesting the nearly amorphous nature of electrode after cycling which is in good agreement with TEM.

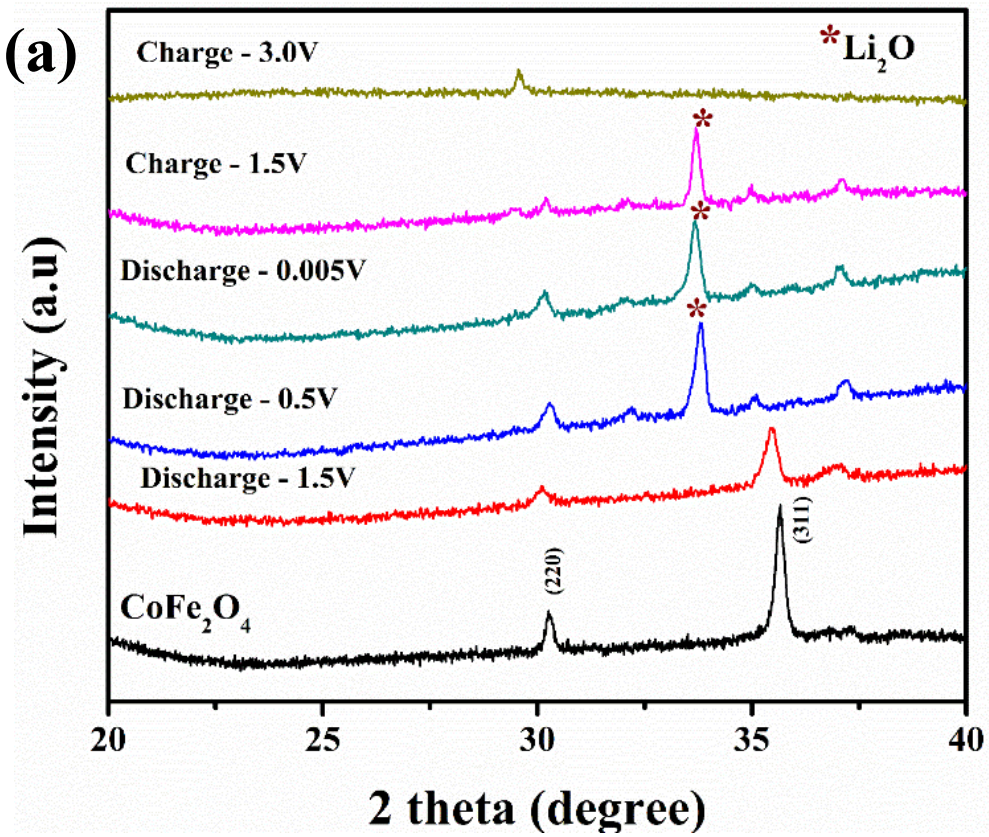
(a)
Charge - 3.0V
*Li2O
Charge - 1.5V
Discharge - 0.005V
Discharge - 0.5V
Discharge - 1.5V
CoFe2O4
(220)
(311)
Intensity (a.u)
20
25
30
35
40
2 theta (degree)

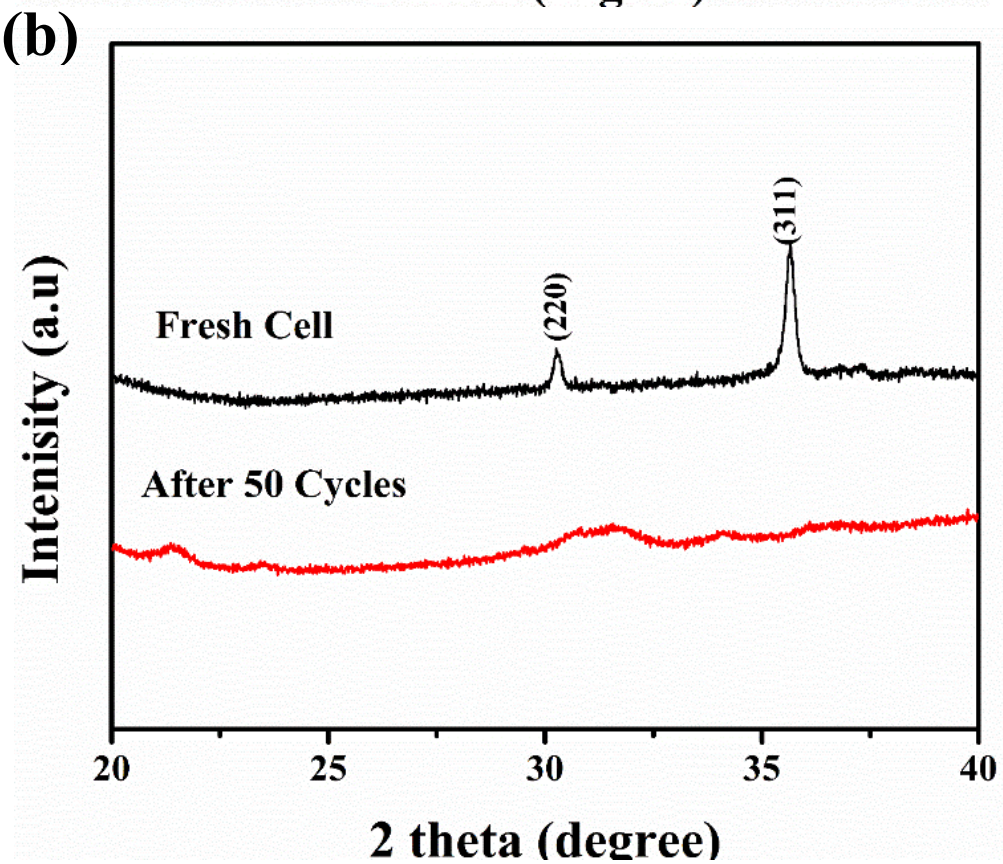
(b)
Fresh Cell
After 50 Cycles
(220)
(311)
Intenisity (a.u)
20
25
30
35
40
2 theta (degree)

Fig.9. (a) Ex-situ X-ray diffraction of $CoFe_2O_4$ at different discharge (1.5 V, 0.5 V and 0.005 V) and charge (1.5 V and 3.0 V) voltages. (b) Ex-situ X-ray diffraction of $CoFe_2O_4$ and the $CoFe_2O_4$ after 50 charge/discharge cycles.

Table 1: Comparison of the electrochemical performance of bare $CoFe_2O_4$ as anode material for lithium ion batteries.

Ref No	Material	Synthesis method	Initial capacity (mAh g^{-1})	Rate studies	Stability
[62]	$CoFe_2O_4$ nanoparticles	Sol-Gel method	--	--	740 mA h g^{-1} after 75 cycles
[63]	$CoFe_2O_4$ nanoplates	De-alloying method	2134 /1415	1280 mAh g^{-1} at 500 mA g^{-1}	810 mA h g^{-1} after 1000 cycles.
[64]	$CoFe_2O_4$ nanofibers	Electrospinning	1278/1236		625 mAh g^{-1} after 100 cycles,
[30]	$CoFe_2O_4$ Spheres	Microwave-hydrothermal reaction	1224/930	720 mAh g^{-1} at 5C	730 mAh g^{-1} after 50 cycles.
[35]	$CoFe_2O_4$ nanosheets	Thermal decomposition	1619/1139	303 mAh g^{-1} at 10 A g^{-1}	448 mAh g^{-1} after 600 cycles
[65]	Mesoporous $CoFe_2O_4$ octahedra	Sol–gel method	1680/1270	366 mA h g^{-1} at 5 A g^{-1}	384 mAh g^{-1} after 3000 cycles.
[39]	Mesoporous $CoFe_2O_4$/CoO nanosheet	Hydrothermal and atomic layer deposition techniques	2468/1705	758 mAh g^{-1} even at 1C	1043 mAh g^{-1} even after 50 cycles
[31]	$CoFe_2O_4$ nanotubes	2 step hydrothermal method	1417/1036	654 mAh g^{-1} at 5000 mA g^{-1}	680 mAh g^{-1} after 500 cycles,
[54]	$CoFe_2O_4$ nanotube	Electrospinning	1228/903	214 mAh g^{-1} at 2 A g^{-1}	831 mAh g^{-1} after 150 cycles
[66]	Hollow $CoFe_2O_4$ nanospheres	Hydrothermal method	2264/1266	1133 mAh g^{-1} at 0.5 *C*	1185 mAh g^{-1} after 50 cycles
[67]	Aggregated $CoFe_2O_4$ nanoparticle	Hydrothermal method	1672/1309	679 mAh g^{-1} at 3.2 A g^{-1}	133 mAh g^{-1} after 120 cycles
Our Work	$CoFe_2O_4$ Nanoparticles	Molten salt method	1556/1093	540 mA h g^{-1} at 1C	369 mA h g^{-1} after 200 cycles

3. Conclusion:

In summary, we have successfully synthesized $CoFe_2O_4$ by low cost, one-pot molten salt method and used it as electrode material for lithium ion batteries. Rietveld analysis shows the pure phase of $CoFe_2O_4$ with crystallite size of 54 nm and SEM as well as TEM images revealed a cube like morphology with average particle size of 115 ± 4 nm; demonstrating that this simple method is capable of achieving pure phase materials in nanostructured form. Cyclic voltammetry showed prominent oxidation/reduction peaks up to 5 cycles which suggests better reversibility of the $CoFe_2O_4$. As an electrode material, the $CoFe_2O_4$ delivered high initial discharge/charge capacity of 1556/1093 mA h g^{-1}. A stable reversible capacity of 926 mA h g^{-1} was obtained at the end of the 30^{th} cycle. Even at high current density of 1 C, a reversible capacity of 540 mA h g^{-1} was obtained showing cyclic stability at high current rates. Ex-situ TEM of the cycled electrodes confirmed the structural breakdown of $CoFe_2O_4$ into CoO and Fe_2O_3. Ex-situ XRD of the electrodes at different charge/discharge voltages showed the structural destruction of $CoFe_2O_4$ at 0.5 V (discharge) and formation of Li_2O, which is expected in conversion-based electrodes. Ex-situ XRD after 50 cycles also shows the structural destruction on cycling explaining the decrease in capacity after cycling. One of the major outcomes is that the synthesis approach is quite simple compared to other synthesis approaches which need sophisticated instruments. All the precursor used in the synthesis are abundant and low cost thus can be scaled up for bulk synthesis for industrial scale.

Acknowledgments:

Rajdeep Singh Rawat and Pranav Kulkarni would like to acknowledge "NIE AcRF Grant RI 4/16 RSR" and NTU-India connect program. Pranav Kulkarni and Geetha Balkrishna wish to acknowledge DST Nanomission Ref. no: SR/ NM/NS-20/2014 for their financial support.

Reference:

[1] C. Julien, A. Mauger, A. Vijh, K. Zaghib, Lithium Batteries: Science and Technology, Springer International Publishing (2015).

[2] A. Mauger, C.M. Julien, J.B. Goodenough, K. Zaghib, Tribute to Michel Armand: From rocking chair - Li-ion to solid-state lithium batteries, J. Electrochem. Soc., 167 (2020) 070507.

[3] M.K. Datta, R. Kuruba, P.H. Jampani, S.J. Chung, P. Saha, R. Epur, K. Kadakia, P. Patel, B. Gattu, A. Manivannan, P.N. Kumta, Electrochemical properties of a new nanocrystalline NaMn2O4 cathode for rechargeable sodium ion batteries, Materials Science and Engineering: B, 188 (2014) 1-7.

[4] M.K. Datta, M. Ramanathan, P. Jampani, P. Saha, R. Epur, K. Kadakia, S.J. Chung, P. Patel, B. Gattu, A. Manivannan, P.N. Kumta, High energy mechano-chemical milling: Convenient approach to synthesis of LiMn1.5Ni0.5O4 high voltage cathode for lithium ion batteries, Materials Science and Engineering: B, 190 (2014) 119-125.

[5] J. Cabana, L. Monconduit, D. Larcher, M.R. Palacin, Beyond Intercalation-Based Li-Ion Batteries: The State of the Art and Challenges of Electrode Materials Reacting Through Conversion Reactions, Adv. Mater., 22 (2010) E170-E192.

[6] M.V. Reddy, M.V.; C.M. Julien, A. Mauger, K. Zaghib, Sulfide and Oxide Inorganic Solid Electrolytes for All-Solid-State Li Batteries: A Review. Nanomaterials 10 (2020) 1606.

[7] M.V. Reddy, A. Mauger, C.M. Julien, A. Paolella, K. Zaghib, Brief history of early lithium-battery development. Materials 13(2020) 1884.

[8] M.V. Reddy, G.V. Subba Rao, B.V.R. Chowdari, Metal Oxides and Oxysalts as Anode Materials for Li Ion Batteries, Chem. Rev., 113 (2013) 5364-5457.

[9] P. Kulkarni, S.K. Nataraj, R.G. Balakrishna, D.H. Nagaraju, M.V. Reddy, Nanostructured binary and ternary metal sulfides: synthesis methods and their application in energy conversion and storage devices, J. Mater. Chem. A, 5 (2017) 22040-22094.

[10] P. Nithyadharseni, K.P. Abhilash, S. Petnikota, M.R. Anilkumar, R. Jose, K.I. Ozoemena, R. Vijayaraghavan, P. Kulkarni, G. Balakrishna, B.V.R. Chowdari, S. Adams, M.V. Reddy, Synthesis and Lithium Storage Properties of Zn, Co and Mg doped SnO2 Nano Materials, Electrochimica Acta, 247 (2017) 358-370.

[11] X. Qi, Z. Yan, Y. Liu, X. Li, G. He, S. Komarneni, Ni and Co doped yolk-shell type Fe 2 O 3 hollow microspheres as anode materials for lithium-ion batteries, Materials Chemistry and Physics, 211 (2018) 452-461.

[12] L. Wang, K. Ding, B. Wei, C. Li, X. Shi, Y. Zhang, X. He, Leaf-like α-Fe2O3 micron-particle: Preparation and its usage as anode materials for lithium ion batteries, Materials Chemistry and Physics, 207 (2018) 58-66.

[13] S. Bao, J. Li, Y. Xiao, P. Li, L. Liu, B. Yue, Y. Li, W. Sun, W. Zhang, L. Zhang, X. Lai, In-situ porous nano-Fe3O4/C composites derived from citrate precursor as anode materials for lithium-ion batteries, Materials Chemistry and Physics, 225 (2019) 379-383.

[14] W. Wang, Y. Liang, Y. Kang, L. Liu, Z. Xu, X. Tian, W. Mai, H. Fu, H. Lv, K. Teng, X. Jiao, F. Li, Carbon-coated SnO2@carbon nanofibers produced by electrospinning-electrospraying method for anode materials of lithium-ion batteries, Materials Chemistry and Physics, 223 (2019) 762-770.

[15] M.N. Moura, R.V. Barrada, J.R. Almeida, T.F.M. Moreira, M.A. Schettino, J.C.C. Freitas, S.A.D. Ferreira, M.F.F. Lelis, M.B.J.G. Freitas, Synthesis, characterization and photocatalytic properties of nanostructured CoFe 2 O 4 recycled from spent Li-ion batteries, Chemosphere, 182 (2017) 339-347.

[16] C. Fu, G. Li, D. Luo, X. Huang, J. Zheng, L. Li, One-step calcination-free synthesis of multicomponent spinel assembled microspheres for high-performance anodes of li-ion batteries: a case study of MnCo(2)O(4), ACS Appl Mater Interfaces, 6 (2014) 2439-2449.

[17] J. Li, J. Wang, X. Liang, Z. Zhang, H. Liu, Y. Qian, S. Xiong, Hollow MnCo2O4 submicrospheres with multilevel interiors: from mesoporous spheres to yolk-in-double-shell structures, ACS Appl Mater Interfaces, 6 (2014) 24-30.

[18] M.V. Reddy, Y. Xu, V. Rajarajan, T. Ouyang, B.V.R. Chowdari, Template Free Facile Molten Synthesis and Energy Storage Studies on MCo2O4 (M = Mg, Mn) as Anode for Li-Ion Batteries, ACS Sustainable Chemistry & Engineering, 3 (2015) 3035-3042.

[19] P. Moni, S. Hyun, A. Vignesh, S. Shanmugam, Chrysanthemum flower-like NiCo2O4-nitrogen doped graphene oxide composite: an efficient electrocatalyst for lithium-oxygen and zinc-air batteries, Chem Commun (Camb), 53 (2017) 7836-7839.

[20] M. Prabu, P. Ramakrishnan, H. Nara, T. Momma, T. Osaka, S. Shanmugam, Zinc-air battery: understanding the structure and morphology changes of graphene-supported CoMn(2)O(4) bifunctional catalysts under practical rechargeable conditions, ACS Appl Mater Interfaces, 6 (2014) 16545-16555.

[21] S. Yuvaraj, A. Vignesh, S. Shanmugam, R. Kalai Selvan, Nitrogen-doped Multi-walled Carbon Nanotubes-MnCo 2 O 4 microsphere as electrocatalyst for efficient oxygen reduction reaction, International Journal of Hydrogen Energy, 41 (2016) 15199-15207.

[22] K.O. Ogunniran, G. Murugadoss, R. Thangamuthu, P. Periasamy, Evaluation of nanostructured Nd0.7Co0.3FeO3 perovskite obtained via hydrothermal method as anode material for Li-ion battery, Materials Chemistry and Physics, 248 (2020).

[23] H.D. Yoo, I. Shterenberg, Y. Gofer, G. Gershinsky, N. Pour, D. Aurbach, Mg rechargeable batteries: an on-going challenge, Energy & Environmental Science, 6 (2013).

[24] S. Li, B. Wang, J. Liu, M. Yu, In situ one-step synthesis of CoFe2O4/graphene nanocomposites as high-performance anode for lithium-ion batteries, Electrochimica Acta, 129 (2014) 33-39.

[25] J. Jiao, K. Du, Y. Wang, P. Sun, H. Zhao, P. Tang, Q. Fan, H. Tian, Q. Li, Q. Xu, N plasma treatment on graphene oxide-MoS2 composites for improved performance in lithium ion batteries, Materials Chemistry and Physics, 240 (2020).

[26] A.I. Mtz-Enriquez, C. Gomez-Solis, A.I. Oliva, A. Zakhidov, P.M. Martinez, C.R. Garcia, A. Herrera-Ramirez, J. Oliva, Enhancing the voltage and discharge times of graphene supercapacitors depositing a CNT/V2O5 layer on their electrodes, Materials Chemistry and Physics, 244 (2020).

[27] Z. Zhang, W. Li, R. Zou, W. Kang, Y. San Chui, M.F. Yuen, C.-S. Lee, W. Zhang, Layer-stacked cobalt ferrite (CoFe2O4) mesoporous platelets for high-performance lithium ion battery anodes, Journal of Materials Chemistry A, 3 (2015) 6990-6997.

[28] M. Zhang, X. Yang, X. Kan, X. Wang, L. Ma, M. Jia, Carbon-encapsulated CoFe2O4/graphene nanocomposite as high performance anode for lithium ion batteries, Electrochimica Acta, 112 (2013) 727-734.

[29] Y. Xiao, X. Li, J. Zai, K. Wang, Y. Gong, B. Li, Q. Han, X. Qian, CoFe2O4-Graphene Nanocomposites Synthesized through An Ultrasonic Method with Enhanced Performances as Anode Materials for Li-ion Batteries, Nano-Micro Letters, 6 (2014) 307-315.

[30] S. Yoon, Facile microwave synthesis of CoFe2O4 spheres and their application as an anode for lithium-ion batteries, Journal of Applied Electrochemistry, 44 (2014) 1069-1074.

[31] X. Zhang, Y. Xie, Y. Sun, Q. Zhang, Q. Zhu, D. Hou, J. Guo, Self-template synthesis of CoFe2O4 nanotubes for high-performance lithium storage, RSC Advances, 5 (2015) 29837-29841.

[32] Y. Zhu, X. Lv, L. Zhang, X. Guo, D. Liu, J. Chen, J. Ji, Liquid-Solid-Solution Assembly of CoFe 2 O 4 /Graphene Nanocomposite as a High-Performance Lithium-Ion Battery Anode, Electrochimica Acta, 215 (2016) 247-252.

[33] M. Zhang, M. Jia, Y. Jin, Q. Wen, C. Chen, Reduced graphene oxide/CoFe2O4–Co nanocomposite as high performance anode for lithium ion batteries, Journal of Alloys and Compounds, 566 (2013) 131-136.

[34] B. Wang, G. Wang, Z. Lv, H. Wang, In situ synthesis of hierarchical CoFe2O4 nanoclusters/graphene aerogels and their high performance for lithium-ion batteries, Physical chemistry chemical physics : PCCP, 17 (2015) 27109-27117.

[35] W. Qi, P. Li, Y. Wu, H. Zeng, L. Hou, C. Kuang, P. Yao, S. Zhou, Facile synthesis of CoFe2O4 nanoparticles anchored on graphene sheets for enhanced performance of lithium ion battery, Progress in Natural Science: Materials International, 26 (2016) 498-502.

[36] P.R. Kumar, P. Kollu, C. Santhosh, K. Eswara Varaprasada Rao, D.K. Kim, A.N. Grace, Enhanced properties of porous CoFe2O4–reduced graphene oxide composites with alginate binders for Li-ion battery applications, New J. Chem., 38 (2014) 3654-3661.

[37] L. Wang, H. Zhao, D. Zhang, W. Song, S. Xu, S. Liu, Z. Li, Ordered mesoporous carbon-supported CoFe2O4 composite with enhanced lithium storage properties, Journal of Materials Science, 52 (2017) 6265-6279.

[38] A.K. Rai, J. Gim, T.V. Thi, D. Ahn, S.J. Cho, J. Kim, High Rate Capability and Long Cycle Stability of Co3O4/CoFe2O4 Nanocomposite as an Anode Material for High-Performance Secondary Lithium Ion Batteries, The Journal of Physical Chemistry C, 118 (2014) 11234-11243.

[39] J. Wang, H. Zhang, X. Lv, K. Nie, X. Gao, J. Zhong, X. Sun, Self-supported ultrathin mesoporous CoFe2O4/CoO nanosheet arrays assembled from nanowires with enhanced lithium storage performance, Journal of Materials Science, 51 (2016) 6590-6599.

[40] P. Afanasiev, C. Geantet, Synthesis of solid materials in molten nitrates. Coord. Chem. Rev. *178*, (1998)1725-1752

[41] X. Liu, N. Fechler, M. Antonietti, Salt melt synthesis of ceramics, semiconductors and carbon nanostructures, Chem Soc Rev, 42 (2013) 8237-8265.

[42] M.V. Reddy, S. Adams, G.T.J. Liang, I.F. Mingze, H. Van Tu An, B.V.R. Chowdari, Low temperature molten salt synthesis of anatase TiO2 and its electrochemical properties, Solid State Ionics, 262 (2014) 120-123.

[43] M.V. Reddy, Z. Beichen, K.P. Loh, B.V.R. Chowdari, Facile synthesis of Co3O4 by molten salt method and its Li-storage performance, CrystEngComm, 15 (2013).

[44] M.V. Reddy, G.V.S. Rao, B.V.R. Chowdari, Synthesis by molten salt and cathodic properties of Li(Ni1/3Co1/3Mn1/3)O2, Journal of Power Sources, 159 (2006) 263-267.

[45] M.V. Reddy, N. Sharma, S. Adams, R.P. Rao, V.K. Peterson, B.V.R. Chowdari, Evaluation of undoped and M-doped TiO2, where M = Sn, Fe, Ni/Nb, Zr, V, and Mn, for lithium-ion battery applications prepared by the molten-salt method, RSC Advances, 5 (2015) 29535-29544.

[46] M.V. Reddy, G.V. Subba Rao, B.V.R. Chowdari, Synthesis and electrochemical studies of the 4V cathode, Li(Ni2/3Mn1/3)O2, Journal of Power Sources, 160 (2006) 1369-1374.

[47] M.V. Reddy, G.V. Subba Rao, B.V.R. Chowdari, Preparation and Characterization of LiNi0.5Co0.5O2and LiNi0.5Co0.4Al0.1O2by Molten Salt Synthesis for Li Ion Batteries, The Journal of Physical Chemistry C, 111 (2007) 11712-11720.

[48] M.V. Reddy, C. Yu, F. Jiahuan, K.P. Loh, B.V. Chowdari, Li-cycling properties of molten salt method prepared nano/submicrometer and micrometer-sized CuO for lithium batteries, ACS Appl Mater Interfaces, 5 (2013) 4361-4366.

[49] M.V. Reddy, L. Yu Tse, W.K.Z. Bruce, B.V.R. Chowdari, Low temperature molten salt preparation of nano-SnO2 as anode for lithium-ion batteries, Materials Letters, 138 (2015) 231-234.

[50] K.S. Tan, M.V. Reddy, G.V.S. Rao, B.V.R. Chowdari, High-performance LiCoO2 by molten salt (LiNO3:LiCl) synthesis for Li-ion batteries, Journal of Power Sources, 147 (2005) 241-248.

[51] X. Zhao, M.V. Reddy, H. Liu, S. Ramakrishna, G.V.S. Rao, B.V.R. Chowdari, Nano LiMn2O4 with spherical morphology synthesized by a molten salt method as cathodes for lithium ion batteries, RSC Advances, 2 (2012).

[52] X. Yao, J. Kong, X. Tang, D. Zhou, C. Zhao, R. Zhou, X. Lu, Facile synthesis of porous CoFe2O4 nanosheets for lithium-ion battery anodes with enhanced rate capability and cycling stability, RSC Adv., 4 (2014) 27488-27492.

[53] C. Yang, X. Ji, X. Fan, T. Gao, L. Suo, F. Wang, W. Sun, J. Chen, L. Chen, F. Han, L. Miao, K. Xu, K. Gerasopoulos, C. Wang, Flexible Aqueous Li-Ion Battery with High Energy and Power Densities, Adv Mater, 29 (2017).

[54] H.-g. Wang, D. Liu, Y. Li, Q. Duan, Single-spinneret electrospinning fabrication of CoFe2O4 nanotubes as high-performance anode materials for lithium-ion batteries, Materials Letters, 172 (2016) 64-67.

[55] Z.H. Li, T.P. Zhao, X.Y. Zhan, D.S. Gao, Q.Z. Xiao, G.T. Lei, High capacity three-dimensional ordered macroporous CoFe2O4 as anode material for lithium ion batteries, Electrochimica Acta, 55 (2010) 4594-4598.

[56] M.V. Reddy, Z. Beichen, L.J. Nicholette, Z. Kaimeng, B.V.R. Chowdari, Molten Salt Synthesis and Its Electrochemical Characterization of Co3O4 for Lithium Batteries, Electrochem. Solid-State Lett., 14 (2011) A79-A82.

[57] M.V. Reddy, C.T. Cherian, K. Ramanathan, K.C.W. Jie, T.Y.W. Daryl, T.Y. Hao, S. Adams, K.P. Loh, B.V.R. Chowdari, Molten synthesis of ZnO.Fe3O4 and Fe2O3 and its electrochemical performance, Electrochim. Acta, 118 (2014) 75-80.

[58] S. Zhao, J. Guo, F. Jiang, Q. Su, G. Du, Porous CoFe 2 O 4 nanowire arrays on carbon cloth as binder-free anodes for flexible lithium-ion batteries, Materials Research Bulletin, 79 (2016) 22-28.

[59] M.V. Reddy, G. Prithvi, K.P. Loh, B.V.R. Chowdari, Li storage and impedance spectroscopy studies on Co3O 4, CoO, and CoN for Li-ion batteries, ACS Applied Materials and Interfaces, 6 (2014) 680-690.

[60] M.V. Reddy, B.L.W. Wen, K.P. Loh, B.V.R. Chowdari, Energy Storage Studies on InVO4 as High Performance Anode Material for Li-Ion Batteries, ACS Appl. Mater. Interfaces, 5 (2013) 7777-7785.

[61] J. Heine, U. Rodehorst, J.P. Badillo, M. Winter, P. Bieker, Chemical Stability Investigations of Polyisobutylene as New Binder for Application in Lithium Air-Batteries, Electrochimica Acta, 155 (2015) 110-115.

[62] P. Lavela, J.L. Tirado, CoFe2O4 and NiFe2O4 synthesized by sol–gel procedures for their use as anode materials for Li ion batteries, Journal of Power Sources, 172 (2007) 379-387.

[63] Z. Wang, P. Fei, H. Xiong, C. Qin, W. Zhao, X. Liu, CoFe 2 O 4 nanoplates synthesized by dealloying method as high performance Li-ion battery anodes, Electrochimica Acta, 252 (2017) 295-305.

[64] Y. Hwangbo, J.-H. Yoo, Y.-I. Lee, Electrospun CoFe2O4 Nanofibers as High Capacity Anode Materials for Li-Ion Batteries, Journal of Nanoscience and Nanotechnology, 17 (2017) 7632-7635.

[65] J. Guo, X. Zhang, Y. Sun, X. Zhang, Mesoporous CoFe2O4 octahedra with high-capacity and long-life lithium storage properties, RSC Advances, 6 (2016) 18-22.

[66] Y. Wang, D. Su, A. Ung, J.H. Ahn, G. Wang, Hollow CoFe(2)O(4) nanospheres as a high capacity anode material for lithium ion batteries, Nanotechnology, 23 (2012) 055402.

[67] J. Mao, X. Hou, X. Wang, S. Hu, L. Xiang, The cubic aggregated CoFe2O4 nanoparticle anode material for lithium ion battery with good performance, Materials Letters, 161 (2015) 652-655.